

Review

The Light-Addressable Potentiometric Sensor and Its Application in Biomedicine towards Chemical and Biological Sensing

Yage Liu ^{1,2}, Ping Zhu ^{1,2}, Shuge Liu ^{1,2} , Yating Chen ^{1,2}, Dongxin Liang ^{1,2}, Miaomiao Wang ^{1,2}, Liping Du ^{1,2,*} and Chunsheng Wu ^{1,2,*} 

- ¹ Department of Biophysics, Institute of Medical Engineering, School of Basic Medical Sciences, Health Science Center, Xi'an Jiaotong University, Xi'an 710061, China; liuyage@stu.xjtu.edu.cn (Y.L.); jewel121@stu.xjtu.edu.cn (P.Z.); 4120115012@stu.xjtu.edu.cn (S.L.); ytc20201011@stu.xjtu.edu.cn (Y.C.); ldx410328@stu.xjtu.edu.cn (D.L.); wmm15029418463@stu.xjtu.edu.cn (M.W.)
- ² Key Laboratory of Environment and Genes Related to Diseases, Xi'an Jiaotong University, Ministry of Education of China, Xi'an 710061, China
- * Correspondence: duliping@xjtu.edu.cn (L.D.); wuchunsheng@xjtu.edu.cn (C.W.)

Abstract: The light-addressable potential sensor (LAPS) was invented in 1988 and has developed into a multi-functional platform for chemical and biological sensing in recent decades. Its surface can be flexibly divided into multiple regions or pixels through light addressability, and each of them can be sensed independently. By changing sensing materials and optical systems, the LAPS can measure different ions or molecules, and has been applied to the sensing of various chemical and biological molecules and cells. In this review, we firstly describe the basic principle of LAPS and the general configuration of a LAPS measurement system. Then, we outline the most recent applications of LAPS in chemical sensing, biosensing and cell monitoring. Finally, we enumerate and analyze the development trends of LAPS from the aspects of material and optical improvement, hoping to provide a research and application perspective for chemical sensing, biosensing and imaging technology.

Keywords: light-addressable potentiometric sensor; LAPS; chemical sensing; biosensing; cell monitoring; sensitivity



Citation: Liu, Y.; Zhu, P.; Liu, S.; Chen, Y.; Liang, D.; Wang, M.; Du, L.; Wu, C. The Light-Addressable Potentiometric Sensor and Its Application in Biomedicine towards Chemical and Biological Sensing. *Chemosensors* **2022**, *10*, 156. <https://doi.org/10.3390/chemosensors10050156>

Academic Editor: Andrey Bratov

Received: 22 March 2022

Accepted: 19 April 2022

Published: 24 April 2022

Publisher's Note: MDPI stays neutral with regard to jurisdictional claims in published maps and institutional affiliations.



Copyright: © 2022 by the authors. Licensee MDPI, Basel, Switzerland. This article is an open access article distributed under the terms and conditions of the Creative Commons Attribution (CC BY) license (<https://creativecommons.org/licenses/by/4.0/>).

1. Introduction

The light-addressable potential sensor (LAPS) is an electrochemical sensing platform based on field-effect capacitor photocurrent measurement. It detects ions and molecules in an electrolyte in a spatially resolved manner. Since its invention in 1988, LAPS has been widely developed and applied for chemical and biomedical research [1]. LAPS is suitable for detecting the potential changes caused by the changes in ion concentrations. It can also be used for the measurement of local impedance (SPIM). It can be based on an electrolyte insulator semiconductor (EIS) or electrolyte semiconductor (ES) substrate. Compared with ion-selective field-effect transistors with interdigital electrodes for measuring conductivity, redox potential or impedance parameters, LAPS combines chemical sensors and optical addressability, and has great potential for electrochemical imaging and biological imaging.

LAPS combines the generation and measurement of photocurrent with the ion environment on the substrate surface. First, we discuss how this combination realizes the measurement and imaging of ion concentration, photocurrent and photovoltage. Further, we use modeling and simulation methods to help explain this process and try to theoretically explain the effects of light source, substrate thickness and doping concentration on the lateral resolution of LAPS. Then, we select and list the applications of LAPS in chemical sensing, biosensing and imaging, along with the improvements in materials and optical systems, in detail, in order to achieve better sensing and imaging process in the future. When

facing different targets of interest, we always need different sensing and imaging strategies according to the actual needs. Figure 1 shows the main advantages of a light-addressable potentiometric sensor compared to other sensors for chemical sensing and biosensing. We illustrate these advantages in detail and discuss the disadvantages of LAPS as well, followed by the challenges faced by today's research and possible solutions. We strongly believe that this review can clarify the current research directions and application methods for LAPS, and help readers use LAPS to develop practical high-resolution biological imaging methods and biosensors with high sensitivity, high selectivity and stability.

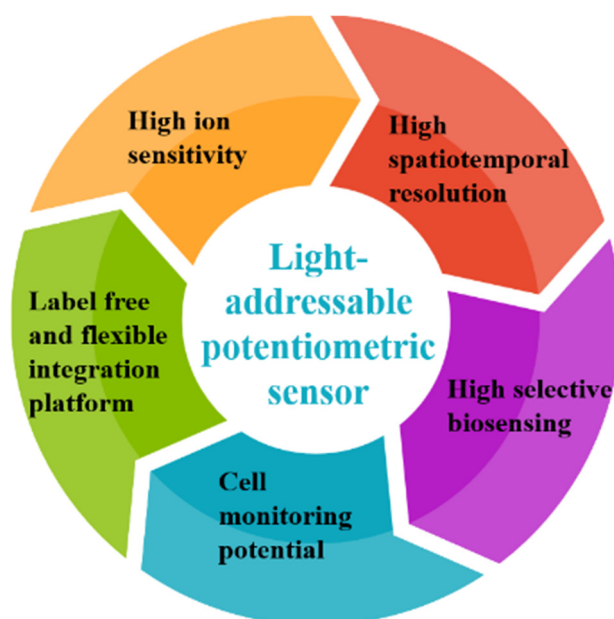


Figure 1. Main advantages of the light-addressable potentiometric sensor.

2. Measurement System of a LAPS

2.1. Principle and Setup

A complete LAPS system includes three basic units: a light source (such as LED or laser beam), a LAPS chip and an electronic circuit for reading photocurrent. For example, Figure 2a shows a typical setup of LAPS based on EIS structure, using culture medium as the electrolyte, $\text{SiO}_2/\text{Si}_3\text{N}_4$ as the insulator, Si as the semiconductor, an LED light source and a constant potential circuit for measurement.

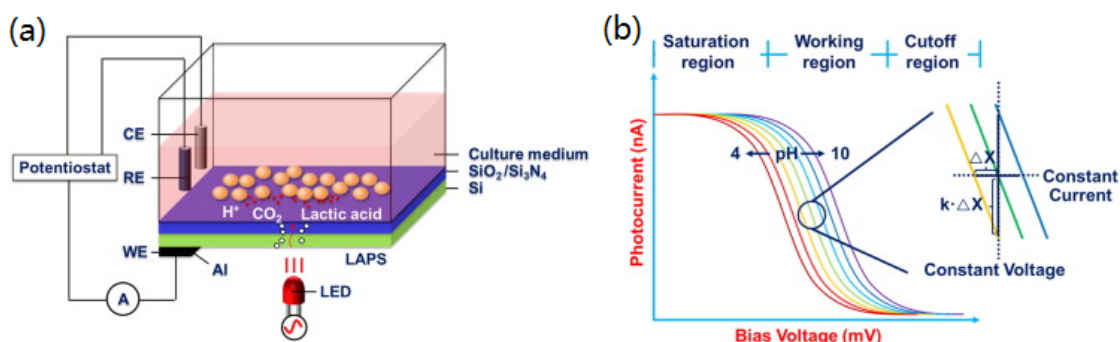


Figure 2. (a) A typical setup of a light-addressable potentiometric sensor for acid detection; (b) typical photocurrent–voltage curves for a LAPS sensor under different pHs, under constant current detection mode and constant voltage detection mode measuring parameters [2].

Most of the carriers are swept away from the surface when a bias voltage is applied to the metal electrode, resulting in a space charge region. When the modulated light is

irradiated on the back of the LAPS through the optical probe, according to band gap theory, that is the internal photoelectric effect. During illumination, electron–hole pairs will be generated on the back surface of the silicon substrate. After the photon-induced carriers are generated, they will begin to diffuse immediately, and some of them will recombine in the path. Only the molecules reaching the space charge region can be bent and separated by the energy band, generating external photocurrent and affecting the spatial resolution. In the absence of light, the excess carriers in the space charge region are released and gradually recombined. Therefore, under modulated illumination, alternating photocurrent can be detected in an external circuit. This is the principle of the LAPS sensing process, and Figure 2b shows typical photocurrent–voltage curves of this process using a constant potential circuit applied to pH sensing.

LAPS devices are optically addressable, which means the signal from each local area (point) on the grid surface can be read by illuminating the area with a modulated light source. This characteristic makes LAPS not only useful for chemical sensing, but also suitable for chemical imaging and multi-sensor applications [1]. When the surface of a semiconductor is scanned by a focused laser beam (scanning setting) or a light source array (e.g., light emitting diode (LED)), the two-dimensional distribution of the change in surface potential caused by the local concentrations of some chemical or biological substances can be detected by measuring the photocurrent at each point.

2.2. Modeling of a LAPS

We know little about the characteristics of the LAPS, even if it has been used in the sensing and imaging of various ions and molecules. For example, it is generally believed that one of the biggest characteristics of a LAPS is its spatial resolution, but so far, the optical characteristics of LAPS devices have not been analyzed in detail. In addition, in an experiment, a LAPS device often cannot obtain a satisfactory spatial resolution and signal-to-noise ratio at the same time, so it is necessary to find a compromise between the two. To reasonably explain these problems, it is essential to establish a LAPS equivalent circuit model to analyze its photocurrent characteristics.

A. Poghosian et al. discussed the impedance effect and crosstalk of a non-illumination area on the measurement of the photocurrent and optical addressability of LAPS devices by designing an extended equivalent circuit model [3]. Photocurrent depends not only on the local interface potential in the illumination area, but also on the possible change in interface potential in the dark area; that is, the change in bypass impedance in the equivalent circuit produces crosstalk effect. In order to minimize the influence of non-illumination area, the experiment proves that when selecting the measuring circuit in the design of LAPS, the input resistance must be much lower than the impedance of the non-illumination area, so that most of the photocurrent flows into the measuring circuit to achieve the best measurement effect.

Tatsuo et al. proposed a circuit model for reflux in LAPS, which is shown in Figure 3 [4]. They discussed the dependence of signal current on various parameters, such as contact area diameter, modulation frequency and solution-specific conductivity, and then calculated the series resistance of the circuit. It was found that due to the differences in reflux in calibration and measurement, the local change in analyte concentration in imaging may be underestimated. In addition, these equivalent circuit models were also used to study the impedance measurements and frequency characteristics of LAPS under different bias voltages. It was found that the input of data acquisition card can be maximized through a three-electrode configuration and a gain scaling network. A better operational amplifier with better noise performance and higher bandwidth can be used to improve the signal-to-noise ratio and bandwidth [5].

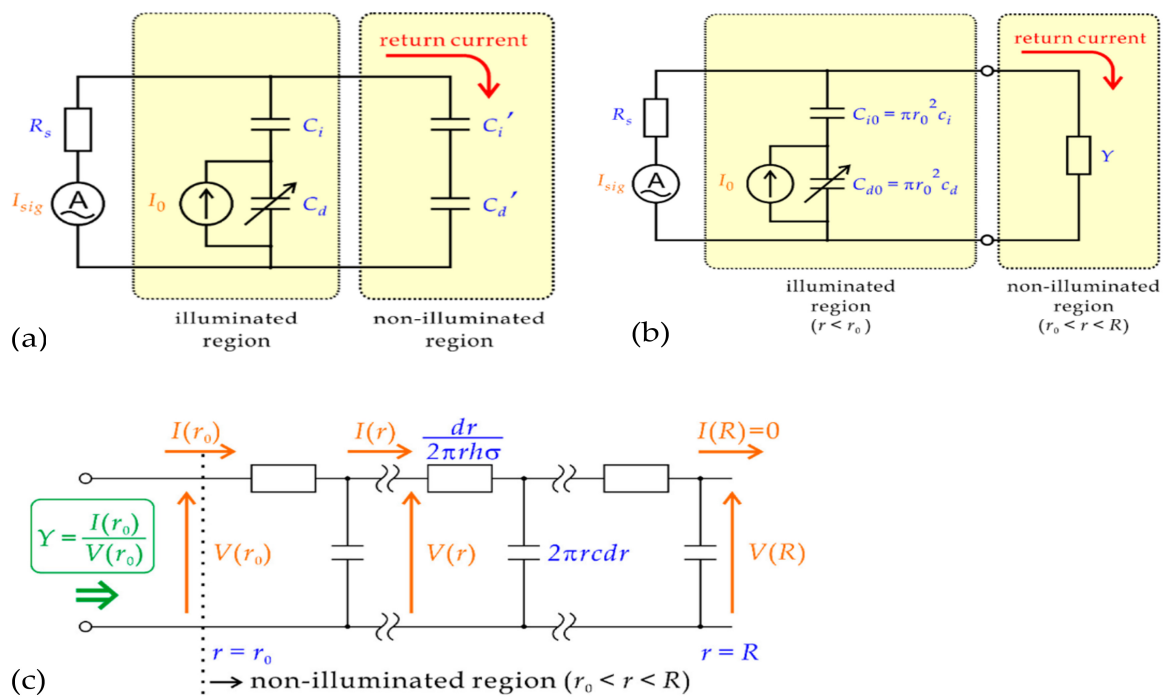


Figure 3. (a) A simple circuit model of the return current; (b) the path of the return current is represented by admittance Y ; (c) a circuit model of the non-illuminated region [4].

2.3. Device Simulation of a LAPS

Differently from establishing the equivalent circuit model, a simplified division simulation is proposed to simulate the carrier distribution and photocurrent response, which provides new insights into the amplitude mode and phase mode operation of LAPS. Similarly, the division simulation also focuses on the spatial resolution of LAPS, which can check various equipment parameters to effectively design and optimize LAPS structure and settings in order to improve performance. By calculating the temporal and spatial variation in electron and hole distribution in semiconductor layer with modulated illumination, the photocurrent response and spatial resolution are obtained. At the same time, the specific relationship between LAPS spatial resolution and substrate thickness, doping concentration and light intensity can be found. Firstly, higher spatial resolution can be obtained by the utilization of a thinner silicon substrate, which can be explained by considering the geometric effect in minority carrier diffusion. Secondly, the spatial resolution is dependent on the minority carrier diffusion length, and the doping concentration has an effect on the minority carrier diffusion length, which is why the doping concentration usually affects the spatial resolution of LAPS in experiments. Third, when the silicon substrate is thick, higher spatial resolution can be obtained using a light source with a longer wavelength and lower illumination intensity. Finally, the simulation results show that the incident angle of constant illumination will also affect the spatial resolution of LAPS, as Figure 4 shows. When combined illumination with large incident angle is used, the spatial resolution can be improved, because the optical carriers are limited near the depletion layer without enhancing the recombination near the back. At this stage, the simulation mainly considers the insulator semiconductor part of LAPS. In the future, it will be necessary to add the electrolyte insulator interface to the division simulation to consider its electrochemical effect [6–8].

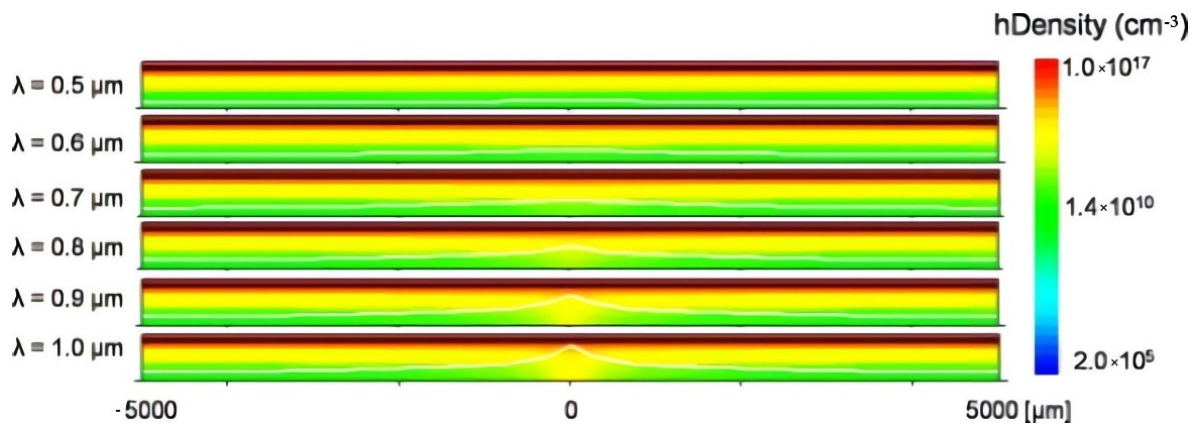


Figure 4. Distribution of minority carriers near the space charge region. The white lines show the border of the space charge region [6].

3. LAPS for Chemical Sensing

3.1. Chemical Sensing and Application

LAPS chemical sensing has been reported for various metal ions by researchers, such as Yoshinobu et al. In the early stage, LAPS combined with a microfluidic system was applied to chemical sensing and imaging at the same time, which was used for the detection of heavy metal ions Pb^{2+} , Cu^{2+} , Cd^{2+} and Hg^{2+} ; and other metal ions, Li^+ , K^+ , CS^+ , Mg^{2+} and Ca^{2+} [9]. LAPS chemical sensing targets are usually heavy metals [10–13], pH [11,14–18], pH imaging [19–24], other metals and nonmetals [9,25–31]. In addition, microfluidics combined with LAPS have been used to monitor ion diffusion for a long time [30]. A LAPS-based method has also been proposed to measure corrosion, combined with biosensor corrosion of materials [18].

Food safety has always been one of the most important application fields of chemical sensors. When detecting video pollutants, SPR and optical biosensors are usually used to detect pesticides, pathogens, heavy metal ions and toxic substances. With the progress in microfluidic and optical technology, the demand for optical biosensors in food safety is increasing. LAPS has been applied to the detection of food safety in recent years, such as heavy metals in fish [12] and Cd content in rice [13]. Figure 5 shows great potential for food safety monitoring using a LAPS. More detailed information of LAPS's application to chemical sensing is shown in Table 1.

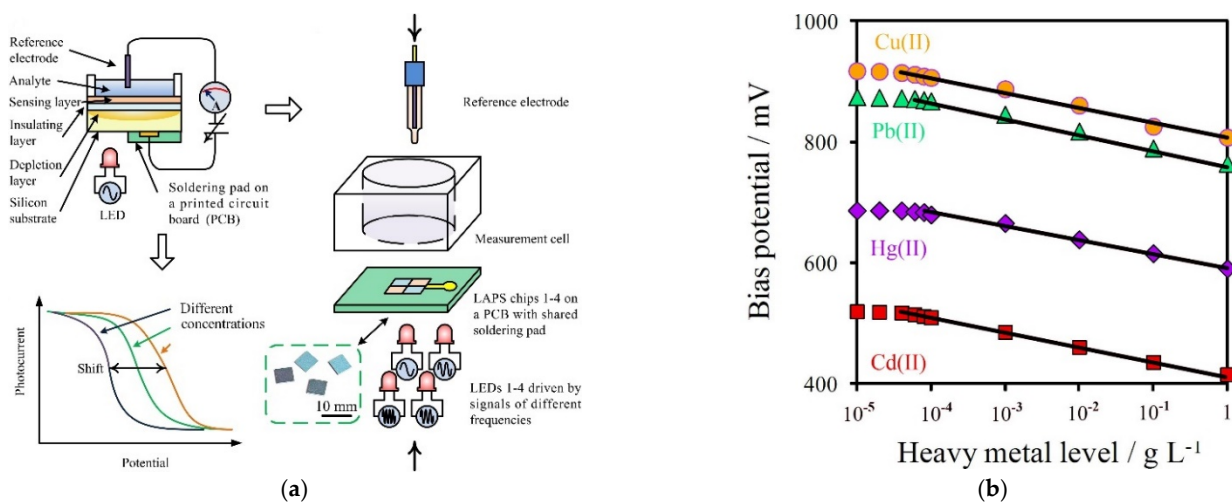


Figure 5. (a,b) A rapid method for the tracing of Cd (II), Pb (II), Cu (II) and Hg (II) in fish tissues [12].

Table 1. Categories, targets, technology, detection limits or ranges, noise and measurement times of articles on LAPS chemical sensing and imaging published in recent years.

Category	Target	Technology	Sensitivity	Detection Limit or Range	Noise	Measurement Time	Ref.
Chemical Sensing	Ions and molecules	LAPS with pulsed laser deposition (PLD)	58 mV/pK, 59 mV/pLi, 57 mV/pCs, 27 mV/pCa and 26 mV/pMg	10 ⁻⁶ –10 ⁻¹ mol/L	-	-	[9]
	pH	LAPS with a HfO ₂ layer	30.1 mV/pH	pH 2–12	-	-	[14]
		LAPS with Gallium nitride (GaN) film	52.29 mV/pH	pH 2–12	-	-	[15]
	Heavy metals	LAPS with PVC membrane	28.7–29.3 mV/dec	10 ⁻⁵ –10 ⁻¹ mol/L	0.5 mV	2–4 s	[10]
	Four taste molecules	LAPS with surface imprinted TiO ₂ membranes	40 ppm/V	2–300 ppm	-	-	[25]
	Ions (pH and heavy metal)	LAPS with a miniaturized multi-sensor chip based on nano-band electrode array (NEA)	0.510 mA/ppb(lead), 0.678 mA/ppb(copper) and 56.49 mV/pH	20–100 ppb	2 mV	120 s	[11]
		LAPS with Microelectrode array (MEA) on the same wafer	36.3 nA/ppb(zinc), 11.2 nA/ppb(lead) and 4.6 nA/ppb(copper) and 52.1 mV/pH	-	4 mV	-	[32]
			-	10 ⁻⁷ –10 ⁻² mol/L (Zn ²⁺ and Pb ²⁺)	-	15 s	[33]
	pH and pNa	LAPS with a HfO ₂ layer	33.9 mV/pNa 31.8 mV/pNa	- -	- -	- -	[16] [17]
	NH ₄ ⁺	LAPS with functionalized ALD-HfO ₂ film	37.28 mV/pNH ₄	-	-	-	[26]
		LAPS with ALD-HfO ₂ films with post RTA and CF ₄ plasma treatment	37 mV/pNH ₄	-	-	-	[27]
	K ⁺ and Cl ⁻	LAPS with ceramic samarium oxide (Sm ₂ O ₃)-sensing membrane	39.21 mV/pK and 36.17 mV/pCl	10 ^{-3.5} –10 ⁰ M	-	-	[28]
	1,5-anhydroglucitol (1,5-AG)	LAPS with gold nanoparticles enhancing enzymatic silver deposition	2.1 mV per gland 1, 5-AG concentration (μg/mL)	40–225 μg/mL	SNR = 3	-	[29]
	Cd(II), Pb(II), Cu(II), Hg(II) in fish tissues	LAPS	-	0.1–1000 mg/L	-	10 s	[12]
	cadmium (Cd) in rice	LAPS with reduced graphene oxide (RGO)	27.9 mV per decade	0.002 mg/L	0.23 mV	10 s	[13]
pH of Crevice Corrosion	LAPS	-	12 μm	-	145 s	[18]	

Table 1. Cont.

Category	Target	Technology	Sensitivity	Detection Limit or Range	Noise	Measurement Time	Ref.
Chemical Imaging	Multi-ion	LAPS with stripe patterns of membranes on the surface	58 mV/pK, 59 mV/pLi, 57 mV/pCs, 27 mV/pCa and 26 mV/pMg	-	-	-	[9]
	pH	LAPS with a commercially available projector	-	pH 5–10	-	15 Hz (22 × 22 μm ²)	[19]
		Phase-mode LAPS	55.7 mV/pH,	pH 4–10	-	-	[20]
		LAPS with digital micromirror device (DMD)	-	-	-	150 ms (500 × 500-pixel image)	[21]
		FDM-LAPS(frequency division multiplex)	-	pH 4–10	-	6.4 s (16 pixels × 128 lines)	[22]
	Ion diffusion	constant-phase-mode operation of the LAPS with EIS	52.7 mV/pH	pH 4–10	-	-	[23]
		LAPS	52.4 mV/pH	pH 4–10	-	24 ms per pixel (128 × 128 pixel image)	[30]
		LAPS with Hybrid Fiber-Optic Illumination	-	68 μm spatial resolution	-	-	[24]
Imaging the impedance of an organic monolayer	LAPS and SPIM	-65 mV potential shift	-	5 mV	15 min (500 × 500 μm ² ; 5 μm step size)	[34]	

3.2. Advanced Materials for Chemical Sensing and Imaging

LAPS chip materials will affect the spatial resolution [35–45], sensitivity [31,35,37,46–50], stability [51], manufacturing simplicity and costs [38,52–54], specific molecular binding ability [55–59], imaging speed [60], super hydrophilic analysis [61] and multi-component analysis ability [62] of LAPS. Therefore, people continue to improve the performances of LAPS devices with new substrate materials and doping methods. For example, Zhou et al. found that as a photocurrent imaging substrate without any modifications, $\text{In}_{0.175}\text{Ga}_{0.825}\text{N}/\text{GaN}$ obtains greater photocurrent under a semiconductor laser, and clearer PMMA dots and photocurrent images of mesenchymal stem cells under a focused laser beam, as shown in Figure 6, giving it greater advantages compared with ITO and ZnO substrates [40].

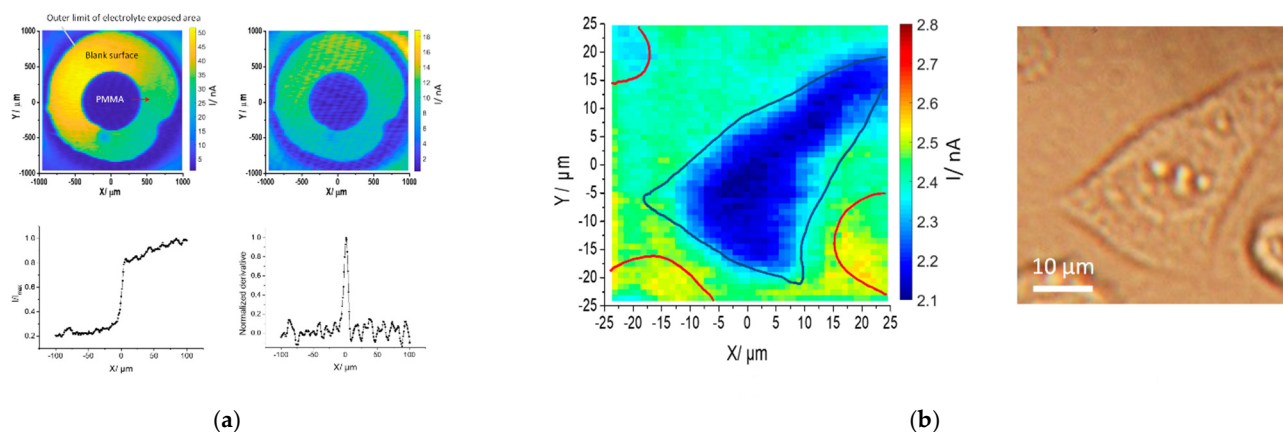


Figure 6. (a) AC photocurrent images of a PMMA dot on InGaN measured at 0.6V; (b) AC photocurrent image of a mesenchymal stem cell on InGaN surface [40].

The LAPS has shown high sensitivity, resolution and imaging speed with various ions and pH levels, since ion and pH measurement became the major application from the very invention of the LAPS. As Table 2 shows, a well designed chemical sensor with LAPS can not only achieve high sensitivity and a low signal-to-noise ratio, but also become a candidate for the development of a biosensor. As we mentioned above, LAPS has great potential for food safety detection, in which the boundary between chemical sensing and biosensing is getting blurred. Therefore, detection of heavy metals and bacteria is suggested to be combined together using LAPS as a platform in the future, but we will face more challenges on specificity, stability and standardization problems.

Table 2. Targets, main improvements, technology, detection limits or ranges, noise and measurement times of articles on the improvements in LAPS chip materials published in recent years.

Target	Main Improvement	Technology	Sensitivity	Detection Limit or Range	Noise	Measurement Time	Ref.
pH	High photocurrent and pH sensitivity	LAPS with thin Si substrate and surface roughness	55.23 mV/pH	pH 2–12	-	-	[35]
	High photovoltage and pH sensitivity	LAPS with thin Si substrate and niobium oxide (NbOx)	60.3 mV/pH	pH 2–10	-	-	[31]
		thin-Si LAPS	45.4 mV/pH	pH 2–12	-	-	[37]
	High-sensitivity imaging and sensing	LAPS using silicon on sapphire (SOS) functionalized with self-assembled organic monolayers	-	49 nA	-	0.01 V/s	[46]
	Improvement on photocurrent and spatial resolution	LAPS with P-I-N amorphous silicon (a-Si) on ITO/glass	40 mV/pH	pH 2–10	-	-	[39]
	Increases of calculated pH sensitivity and linearity	LAPS with a niobium oxide (NbOx) layer	60 mV/pH	pH 3–10	0.3 mV	-3 mV/h	[47]
	pH sensing membrane	LAPS with fluorographene sensing membrane	56.8 mV/pH	pH 2–12	-	2.6 mV/h	[48]
		LAPS with In–Ga–Zn oxide (IGZO) layer	61.8 mV/pH	pH 2–12	-	-	[49]
	Low cost and robust	LAPS and SPIM using ITO-Coated glass as the Substrate Material	70 mV/pH	2.3 μ m resolution	-	-	[54]
	Increase AC photocurrent with enhanced image resolution	LAPS with ZnO Nanorods as the Sensor Substrate	53 mV/pH	45.7 nA photocurrent	0.1 nA	6 h stability	[41]
	Higher photovoltage	LAPS with niobium oxide (NbOx)/P-I-N amorphous silicon (a-Si) on ITO/glass structure	40 mV/pH	pH 2–10	-	-	[42]
	Higher photocurrent and high speed imaging	LAPS with Inductively coupled plasma reactive-ion etching (ICP-RIE) (Si substrate)	55.8 mV/pH	pH 2–12	-	-	[60]
	Higher photovoltage	LAPS with In–Ga–Zn oxide (IGZO) semiconductor layer	66 mV/pH	pH 2–12	-	-	[43]

Table 2. Cont.

Target	Main Improvement	Technology	Sensitivity	Detection Limit or Range	Noise	Measurement Time	Ref.
	pH sensing evaluation	LAPS with SnOx as a photosensitive semiconductor	1.29 μ A and 57.6 mV/pH	pH 4–10	-	-	[50]
	Low cost and high performance	LAPS with well-ordered polystyrene (PS) colloidal monolayer	53.47 mV/pH	pH 4–10	-	-	[63]
	High spatial resolution, high speed imaging and high signal-to-noise ratio	LAPS with anisotropic etching process based on tetramethylammonium hydroxide (TMAH)	-	20 μ m spatial resolution	-	10 Hz–120 kHz	[44]
	High photocurrent and immunity to room light inference	LAPS with Indium Gallium Zinc Oxide (IGZO) on Indium Tin Oxide (ITO) glass (IGZO LAPS)	58.9 mV/pH	pH 2–12, 50 μ m pattern recognition s	-	-	[45]
	Superhydrophilic	LAPS with Plasma Treatment	59.6 mV/pH	pH 6–10	4 mV hysteresis	117 h	[61]
Neurons (from rat embryos)	Compatibility and easy to fabricate	LAPS using TiO ₂ as a photo-conductor	10 μ C/cm ² /V	-	-	5 min	[52]
photocurrent	No need to apply DC bias voltage and for gas detection	LAPS with silicon p–n junction from solar cell	-	-	-	10 ³ cm/s	[53]
	Immobilizing enzymes	LAPS with quantum dots as switchable layer	-	913 nA	-	-	[55]
DNA	Resist nonspecific adsorption to the DNA-modified interface on Si(100) devices	LAPS and light-addressable amperometric sensors based on organic-monolayer-protected Si(100)	-	1.0×10^{-11} – 1.0×10^{-6} M DNA	4.5%STD	-	[57]
No specific target	AC photoelectrochemical imaging	LAPS with InGaN/GaN thin films	-	10 nm narrow gap	-	-	[40]
	Flexibility and resolution of the image	LAPS with mini-projector and miniaturized amorphous-silicon	-	72 μ m \times 72 μ m spot size	SNR = 10.72	-	[38]
	Impedance of functionalized microcapsules	LAPS with microcapsules modified with gold nanoparticles	-	20 μ m \times 25 μ m spot size	-	-	[59]
	Repair thermally grown oxide layers	LAPS and SPIM	-	1.31 nA/cm ²	-	-	[56]

Table 2. Cont.

Target	Main Improvement	Technology	Sensitivity	Detection Limit or Range	Noise	Measurement Time	Ref.
	Characterization	LAPS with chemically patterned non-oxide SOS substrate	−50 mV voltage shift	-	-	-	[58]
	Keep the electrode stable longer	LAPS with Perhydropolysilazane-Derived Silica Treated by O ₂ Plasma (passivation)	-	-	-	100 h stability	[51]

4. LAPS for Biosensing

4.1. Biosensing and Imaging

A biosensor using LAPS uses enzymes [19,38,64], antigens or antibodies [65–67], DNA [68–71], cells [72–76], sensitive materials [77–80] or biological initiators [81] to detect specific biochemical molecules of interest, which greatly expands the detection range of LAPS and generally provides good specificity, as shown in Table 3. In addition, the rapid detection of LAPS can overcome the disadvantage of poor binding stability between the LAPS chip and biomolecules or cells to a certain extent.

4.2. Cell Monitoring

A LAPS has the ability to characterize the chemical processes of cells cultured on the LAPS's surface, which is a unique advantage of LAPS among electrochemical sensors. As a result, people can use LAPS for monitoring and imaging of cell metabolism. The target cells monitored in recent studies were rat renal cells [87–89], cardiac myocytes [90,91], human breast cancer cells [2], mouse embryonic fibroblasts [92], *Escherichia coli* [65,93–96], HeLa cell lines [97], Chinese hamster oval (CHO) cells [25,96,98,99], adrenal chromaffin cells [100], C3 cells [99], *Corynebacterium glutamicum* [93,94], *Lactobacillus brevis* [93,94,101], MDA MB231 and MDA-MB-435MDR [102] and hepatoma HepG2 cells [103]. Stimulated cells have also been reportedly monitored by LAPS [84,85,104,105]. On this basis, LAPS cell monitoring was further applied to in vivo pH probes [106], deep brain recordings [107] and detection of cells [108–111].

LAPS can realize more effective monitoring of cell activities, especially high-speed monitoring of cell metabolites, cell responses to different targets and the extracellular environment in a label free sensing process, which can hardly be achieved by other optical imaging or chemical sensing methods. However, the biosensing processes, especially cell monitoring, are limited mainly because of the low biocompatibility of LAPS chips and the difficulty of raising photocurrent and spatial resolution with materials and optical methods. The imaging times are too long to get more detailed information of cell activities as well, according to Table 4. Therefore, for the development of biosensors using LAPS, we should continually focus on achieving higher photocurrent, spatial resolution and scanning speed, and better stability and biocompatibility. More aspects of cell interaction with LAPS chips and electrolyte and optical systems should be considered in the development of biosensors using LAPS.

Table 3. Categories, targets, technology, sensitivities, detection limits or ranges, noise and measurement times of articles on LAPS biosensing and imaging published in recent years.

Category	Target	Technology	Sensitivity	Detection Limit or Range	Noise	Measurement Time	Ref.
Enzyme-based biosensor	Urease	LAPS with an enzyme reactor in a fluidic channel	-	0.3×10^{-3} – 10^{-1} mol/L	-	12.5 μ L/min	[82]
	Glucose oxidase	LAPS with on-board light driver and transimpedance amplifier	101.1 mV/dec	0.01–100 mM	-	10 s	[83]
Affinity-based biosensor	Short chain single strand DNA (ssDNA)	GO-LAPS (Graphene oxide (GO) based LAPS)	-	1 pM–10 nM	-	50 mV/s	[69]
		LAPS	-	100 mV	-	-	[70]
		LAPS with different ssDNA chains	0.514 mV/lg[ppb]	0.01–100 ppb	3.9%STD	-	[71]
	DNA sequences related to HBV, HCV, HIV	LAPECS	0.29 μ A/logC(nM)	0.7 pM	0.7 μ A	-	[72]
	Functional Nucleic Acids	FNA-LAPS	2.86 (Pb ²⁺) and 1.53 (Ag ⁺) mV/lg(ppb) 0.39 \pm 0.07 pA per ng/mL, 0.22 \pm 0.04 pA per ng/mL,	0.01 ppb	-	30 min	[80]
	Antigens and antibodies of AFP CEA CA19-9 Ferritin	LAPS with chip initiated by L-Dopa	0.18 \pm 0.07 pA per U/mL and 0.12 \pm 0.02 pA per 10 ng/mL for AFP, CEA, CA19-9 and Ferritin	20 ng/mL(AFP)	-	-	[67]
	Human immunoglobulin G (hIgG)	LAPS with goat anti-human immunoglobulin G antibody	$\Delta V(V) = 0.00714$ $C_{hIgG}(\mu g/mL) - 0.0147$	0.15 μ g/mL	SNR = 3	-	[68]
	Mouse IgG detecting rabbit anti-mouse IgG	LAPS	65.7 μ V/p[IgG]	0.01 μ g/mL	-	-	[66]
5-methylcytosine (5mC)	LAPS with DNA Methylation Sensing Interface	-	10 pM–100 nM	-	-	[78]	

Table 3. Cont.

Category	Target	Technology	Sensitivity	Detection Limit or Range	Noise	Measurement Time	Ref.	
	Alpha-fetoprotein (AFP)	LAPS with gold nanoparticles (Au NPs)	2.5892 mV/ μ g/mL	92.0 ng/mL	2.76%RSD	-	[81]	
	Circulating-tumor-cell (CTC)	LAPS with porous-graphene-oxide (PGO) enhanced aptamer specific CTC sensing interface	$\Delta V_{out}/V_{out,0} = -7.63, -9.85, -6.67\%/lg[\text{spiked cells}]$ for A549, HeLa and MDAMB231	5–5000 spiked cells	-	30 min	[79]	
Cell-based biosensor	Heavy metal	MLAPS with stripping voltammetry	-	280 μ g/L Fe(III), 26 μ g/L Cr(VI)	-	0.02 V/s	[73]	
	Tastants mixture	LAPS	-	10–30 μ V	-	-	[84]	
	Nutrient concentration	LAPS	(89.0 \pm 1.5) mV per decade glucose	0.5 mM glucose	-	-	[74]	
	Odorants or neurotransmitters	LAPS	-	1 μ M acetic acid	-	-	[75]	
				-	25 μ V	-	-	[76]
				-	45 μ V	-	60 s	[77]
	HCl	LAPS in both time domain and frequency domain	-	pH 2–7.5	SNR = 3	-	[85]	
Bio-initiator-based biosensor	L-DOPA for protein binding and immunoassay	LAPS with the surface bio-initiated by L-DOPA	5.68 nA/p[Ag]	0.001–4 μ g/mL IgG	-	-	[82]	
	Polyion-based enzymatic membrane for acetylcholine (ACh)	LAPS and CCD	56.5 mV/pH for LAPS and 20.5 mV/pH for CCD-type sensor	1 μ M–1 M ACh	-	200 ms/frame	[86]	

Table 4. Categories, targets, technology, sensitivities, detection limits or ranges, noise and measurement times of articles on LAPS cell monitoring published in recent years.

Category	Target	Technology	Sensitivity	Detection Limit or Range	Noise (mV)	Measurement Time	Ref.
Cell metabolism	Rat renal cells	LAPS with heavy doping and thick oxide layer	56.99 mV/pH	64% ECAR (extracellular acidification rate)	5 nA	-	[87]
		LAPS with an electrolyte-insulator-semiconductor (EIS)	41.6 mV/pH	-	-	-	[88]
		LAPS with electrical cell-substrate impedance sensor (ECIS)	57.7 mV/pH	24% ECAR	-	2.5 h	[89]
		LAPS with EIS (impedance measurement)	$7.87 \pm 1.90\%$ (RMS \pm standard deviation)	-	-	30 min	[37]
	Cardiac myocytes	LAPS	53.9 mV/pH	-	0.25 mV	90 ms (extracellular potential)	[90]
		LAPS and ECIS	1 nA	-	-	1.0×10^{-4} s (time resolution)	[91]
		Four-channel LAPS	-	20–40 μ V	-	30 to 250 times per min (beating frequencies)	[104]
	Human breast cancer cells MCF-7	LAPS with constant voltage detection mode	1104 nA/pH	80% ECAR	1 nA	-	[2]
	Mouse embryonic fibroblast 3T6 cells	LAPS and cellular impedance sensor(LAPCIS)	-	0.16 CI (in cell index), 9.3% ECAR	-	24–48 h	[92]
	<i>Escherichia coli</i> (<i>E. coli</i>)	LAPS with polyacrylamide gel	5.0×10^4 H ⁺ s ⁻¹ per cell	-	0.06 mV	36–48 min	[112]
Chinese hamster ovary (CHO) cells	LAPS	52.8 mV/pH	0.24 mV/min	-	10 min	[99]	
	LAPS with polymer (PP-ABS) multi-chamber structure	-	2.9 mV/min	-	-	[98]	
	LAPS with multi-chamber structures	54 mV/pH	2.78 mV/min	-	-	[96]	
	LAPS with microfluidic unit	56 mV/pH	0.79 mM/pH (buffer capacity)	-	5 h	[25]	

Table 4. Cont.

Category	Target	Technology	Sensitivity	Detection Limit or Range	Noise (mV)	Measurement Time	Ref.
	Adrenal chromaffin cells	LAPS	-	15% ECAR	20 dB (SNR)	10 min	[100]
	C3 cells	LAPS	-	17–299 mM (glucose concentration)	-	30 min	[99]
	<i>Escherichia coli</i> , <i>Corynebacterium glutamicum</i> , and <i>Lactobacillus brevis</i>	Differential LAPS	54 mV/pH	1.7–400 mM (glucose concentration)	0.02 mV	30 min	[113]
			0.5 mV/min	1.67 mM (glucose concentration)	0.02 mV	40 min	[94]
	HeLa cell lines	LAPS and ECIS	52.88 mV/pH	20% ECAR	-	24 h	[97]
	Cancer cells (MDA MB231 and MDA-MB-435MDR)	LAPS with pH sensitive hydrogel nanofibers (NF-LAPS)	74 mV/pH	-	5 nA	90 min	[102]
	Hepatoma HepG2 cells	LAPS with Microfluidic chip system	335.5 nA/pH	17.88 mpH/min	-	17 min	[103]
	<i>Corynebacterium glutamicum</i> (C. glutamicum ATCC13032)	LAPS with multi-chamber structures	54 mV/pH	0.22 mV/min	0.03 mV	2 nm/s	[101]
	<i>Escherichia coli</i> K12 (<i>E. coli</i> K12)	LAPS with with multi-chamber structure	54 mV/pH	0.55 mV/min	-	60 min	[95]
			-	1.97 mV/min	0.05 mV	20 min	[96]
	Taste receptor cells (from Sprague–Dawley rat)	LAPS in both time domain and frequency domain	-	-	10 dB (SNR)	49.65 ± 1.92 ms (extracellular potential)	[85]
	Rat taste bud cells	LAPS	-	10–30 µV	-	-	[114]
		LAPS and platinum electrodes	-	0.8% (signal change)	-	30 min	[105]
Detection of cells	Mammary adenocarcinoma cell (MDAMB231)	Phage-LAPS	-	10–60 µV	-	-	[108]
	<i>Escherichia coli</i> Detection in Orange Juice	Portable nanofiber LAPS (NF-LAPS)	0.149 per CFU/mL	10 ² –10 ⁶ CFU/mL	-	60 min	[109]
	<i>E. coli</i>	NF-LAPS	74 mV/pH	20 CFU/ml	0.003 mV	60 min	[110]
	CTC	LAPS with anti-EpCAM on carboxylated graphene oxide (GO-COOH)	-	5–1281 CTCs/ml	-	-	[111]

Table 4. Cont.

Category	Target	Technology	Sensitivity	Detection Limit or Range	Noise (mV)	Measurement Time	Ref.
pH probe in vivo	Hippocampal formation of rats	LAPS with a multimodal fiber fabricated by the convergence thermal drawing	57.5 mV/pH	250 μm (spatial resolution)	2.2 mV	30 Hz (temporal resolution), 14 pixels simultaneously	[106]
Deep brain recordings	Mouse hippocampus	LAPS	50 mV/pH	$5 \pm 1.5 \Omega/\text{cm}$	0.8 dB/cm	200 Hz	[107]

5. Optical System Improvements for LAPS

Higher lateral resolution, sensitivity, stability, measurement and imaging speed are the main improvements achieved by improving the optical system of a LAPS. These improvements include light sources [64], optical devices, optical control systems, etc. For example, Zhou et al. proposed a new high-spatio-temporal resolution photoelectrochemical imaging system (PEIS) which uses an analog micromirror to obtain a diffraction-limited laser spot to scan the sensor's surface (see Figure 7a). The multifunctional system is based on an electrolyte insulator semiconductor (EIS). This structure achieves very fast LAPS measurements and high-speed AC/DC photoelectrochemical imaging based on its electrolyte semiconductor (ES) structure, along with high lateral resolution. The use of PEIS makes the details of cell viability clearer than with a typical fluorescence microscope. In addition, EIS can image multiple cells simultaneously and continuously, and monitor the concentrations of ions and metabolites at the same time, as shown in Figure 7b, which provides electrochemical information that other electrochemical imaging devices do not [115]. Miyamoto et al. used mixed illumination composed of a modulated beam and annular constant illumination to suppress the transverse diffusion of optical carriers through enhanced recombination [116]. The spatial resolution of the chemical imaging sensor has been improved and can distinguish chemical images of $100\ \mu\text{m}$. More detailed information of overall progress by improving optical system for LAPS is shown in Table 5.

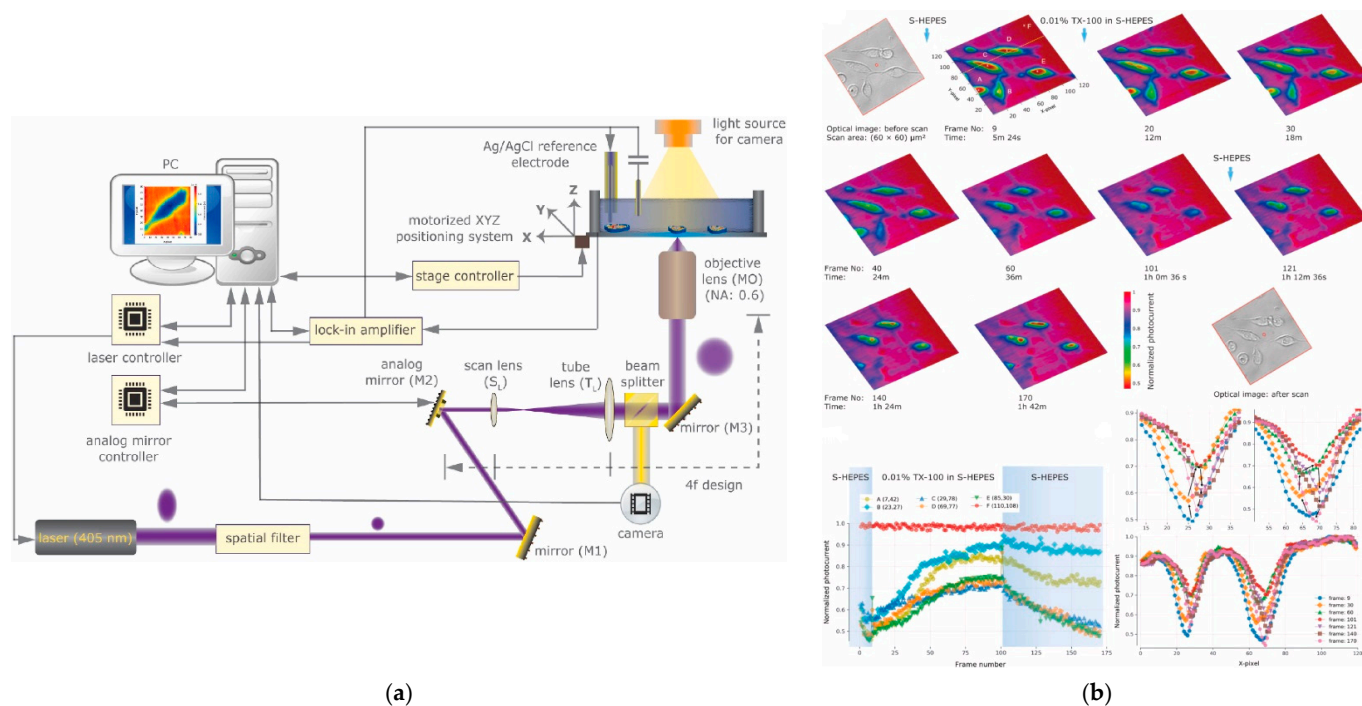


Figure 7. (a) Schematic of the photoelectrochemical imaging setup with an analog micro-mirror-based fast beam steering was achieved with 4f design lens relay system. (b) Photocurrent changes under cells during exposure to a TX-100 concentration smaller than the critical micelle concentration. Including time-lapse photocurrent images of B50 cells exposed to 0.01% TX-100 in S-HEPES buffer, time-dependent photocurrent traces for individual cells and photocurrent X-axis line scan analysis [115].

Table 5. Targets, main improvements, technology, detection limits or ranges, noise and measurement times of articles on the improvement of LAPS optical systems published in recent years.

Target	Main Improvement	Technology	Sensitivity	Detection Limit or Range	Noise	Measurement Time	Ref.
pH	Resolution of the image	LAPS with an OLED display	53.7 mV/pH	pH 4–10	-	1536 s (1.6 mm × 1.6 mm, spot size of 200 μm)	[101]
	High-speed chemical imaging	LAPS by frequency division multiplex (FDM)	0.26/pH (normalized photocurrent)	pH 4–10	-	70 frames per second	[104]
	Suppress lateral diffusion of photocarriers	LAPS with ring-shaped constant illumination	-	100 μm spatial resolution	-	-	[116]
	Lateral resolution enhancement	pulse-driven LAPS	53.5 mV/pH	pH 5–10	0.2 mV	1.5 ms per spot (spot size of 100 μm)	[117]
	Higher spatial resolution	LAPS with a novel photoexcitation method	-	82.32 μm spatial resolution	-	-	[118]
	High measurement resolution and miniaturisation, reduces measurement time	LAPS with an OLED display (new developed driving method)	58 mV/pH	pH 5–9	-	25 ms per spot (spot size of 200 μm)	[119]
	Eliminate measurement error caused by fluctuation, distortion and noise of light source output	LAPS with a SLED	54.8 mV/pH	pH 5–9	7 mV	50 s	[120]
	Increasing the measurement spot density	LAPS using VCSEL array and FPGA (field-programmable gate array) control)	59.9 mV/pH	pH 4–9	-	14 ms per spot	[121]
	High-speed measurement and flexibility of addressing	LAPS using an analog micromirror (back side)	50.4 mV/pH	pH 2–12	-	40 s (14.5 × 10.5 mm ² , 16 fps)	[122]
	Easy, flexible, and miniaturized light source	LAPS with LCD projector	53 mV/pH	pH 1.9–9.14	0.27 mV	20 Hz (spot size of 180 μm)	[123]
	Better linearity and accuracy	LAPS with a superluminescence LED (SLED)	52.5 mV/pH	pH 3–11	7 mV	150 Hz	[124]
	Reduces the size of the set-up and increases the stability and speed of the measurement	LAPS based on the digital light processing (DLP)	-	pH 7	-	0.39 ms per spot (step width of 43 μm, spot size of 130 μm)	[125]

Table 5. Cont.

Target	Main Improvement	Technology	Sensitivity	Detection Limit or Range	Noise	Measurement Time	Ref.
	Simultaneous stimulation of several areas	Multi spot LAPS with FPGA based controller and integrated signal correction mode	57 mV/pH	pH 7–9	3 mV	200 ms	[126]
	Large chemical images	LAPS with digital mirror device (DMD)	-	-	-	11 ms per spot (spot size of 130 μm)	[127]
	Increase the number of measurement spots, shorten time and improve accuracy	LAPS with FPGA	54.6 mV/pH	pH 4–9	1.4 mV	-	[128]
	High resolution and sensitivity	LAPS and SPIM using SOS substrates with a thin anodically grown oxide illuminating the back of the semiconductor substrate	-	0.8 μm resolution	0.1 μm	-	[129]
	Improving signal-to-noise ratio (SNR)	LAPS with optical focusing	-	pH 4–9	-	-	[130]
<i>Escherichia coli</i> (<i>E. coli</i>) K12	Reduce scattering effects	Multi-Chamber LAPS with FPGA-Controlled Laser-Diode Modules	54 mV/pH	0.3×10^9 – 4.8×10^9 cells	0.15 mV	5.60 mV/min (4.8×10^9 cells)	[131]
B50 rat neuroblastoma cells	High speed, lateral resolution and photocurrent stability	LAPS with analog micromirror and $\alpha\text{-Fe}_2\text{O}_3$ (hematite) thin films	23 mV/pH	-	-	8 fps	[115]

6. Conclusions

LAPS has great application prospects in chemical and biomedical sensing and imaging, but many new problems have emerged. There are many problems and challenges to be solved for emerging chemical materials: the affinity and stability of biomaterials combined with LAPS chips, and physical simulation and optical system construction. Both chemical sensors and biosensors based on LAPS are facing the challenge of difficulties improving sensitivity, selectivity and detection limits in time and space, including photocurrent, special resolution and speed of imaging. The difference is that chemical sensors care more about sensitivity, whereas specificity, stability and biocompatibility are highly valued in the development of biosensors. In the future, the abiotic parts of a LAPS could be considered as a whole system in the device simulation process, combining the electrolyte insulator interface with the insulator semiconductor part of a LAPS and optical system during sensor developing and data processing. It is predictable that the developments in electrodes and optical systems will provide higher photocurrents and imaging speeds for LAPS. Integrating the field-effect charge sensing process in LAPS with microfluidic technologies could further improve the sensitivity and accuracy. Moreover, more strategies for interface functionalization of biomacromolecule and cell culturing should be used to take more advantage of the light addressability in biosensing process. At the same time, miniaturization and performance improvements are being carried out, which may allow more applications in biomedicines.

Author Contributions: Y.L.: Conceptualization, Writing—Original draft preparation; P.Z.: Writing—Review and Editing, Visualization; S.L.: Writing—Review and Editing, Visualization; Y.C.: Writing—Review and Editing; D.L.: Writing—Review and Editing; M.W.: Conceptualization, Writing—Review and Editing; L.D.: Conceptualization, Writing—Review and Editing, Supervision, Funding acquisition; C.W.: Writing—Review and Editing, Supervision, Funding Acquisition, Project Administration. All authors have read and agreed to the published version of the manuscript.

Funding: This work was financially supported in part by grants from the National Natural Science Foundation of China (grant numbers 32071370, 51861145307, and 31700859), and the Key Research and Development Program of Shaanxi Province—International Science and Technology Cooperation General Project (grant number 2022KW-23).

Institutional Review Board Statement: Not applicable.

Informed Consent Statement: Not applicable.

Data Availability Statement: Not applicable.

Conflicts of Interest: The authors declare that they have no known competing financial interest or personal relationships that could have influenced the work reported in this paper. The authors declare no conflict of interest.

References

1. Dean, G.; Hafeman, J.; Wallace, P.; Harden, M.M. Light-Addressable Potentiometric Sensor for Bio-chemical Systems. *Science* **1988**, *240*, 1182–1185.
2. Hu, N.; Wu, C.; Ha, D.; Wang, T.; Liu, Q.; Wang, P. A novel microphysiometer based on high sensitivity LAPS and microfluidic system for cellular metabolism study and rapid drug screening. *Biosens. Bioelectron.* **2012**, *40*, 167–173. [[CrossRef](#)] [[PubMed](#)]
3. Yoshinobu, T.; Miyamoto, K.I.; Werner, C.F.; Poghossian, A.; Wagner, T.; Schoning, M.J. Light-Addressable Potentiometric Sensors for Quantitative Spatial Imaging of Chemical Species. *Annu. Rev. Anal. Chem.* **2017**, *10*, 225–246. [[CrossRef](#)] [[PubMed](#)]
4. Yoshinobu, T.; Sato, D.; Guo, Y.; Werner, C.F.; Miyamoto, K.-I. Modeling of the Return Current in a Light-Addressable Potentiometric Sensor. *Sensors* **2019**, *19*, 4566. [[CrossRef](#)]
5. Werner, C.F.; Wagner, T.; Yoshinobu, T.; Keusgen, M.; Schoening, M.J. Frequency behaviour of light-addressable potentiometric sensors. *Phys. Status Solidi* **2013**, *210*, 884–891. [[CrossRef](#)]
6. Guo, Y.; Miyamoto, K.-I.; Wagner, T.; Schöning, M.J.; Yoshinobu, T. Device simulation of the light-addressable potentiometric sensor for the investigation of the spatial resolution. *Sens. Actuators B Chem.* **2014**, *204*, 659–665. [[CrossRef](#)]
7. Guo, Y.; Seki, K.; Miyamoto, K.-I.; Wagner, T.; Schöning, M.J.; Yoshinobu, T. Device Simulation of the Light-addressable Potentiometric Sensor with a Novel Photoexcitation Method for a Higher Spatial Resolution. *Procedia Eng.* **2014**, *87*, 456–459. [[CrossRef](#)]

8. Guo, Y.; Miyamoto, K.-I.; Wagner, T.; Schoening, M.J.; Yoshinobu, T. Theoretical study and simulation of light-addressable potentiometric sensors. *Phys. Status Solidi* **2014**, *211*, 1467–1472. [[CrossRef](#)]
9. Yoshinobu, T.; Iwasaki, H.; Ui, Y.; Furuichi, K.; Ermolenko, Y.; Mourzina, Y.; Wagner, T.; Näther, N.; Schöning, M. The light-addressable potentiometric sensor for multi-ion sensing and imaging. *Methods* **2005**, *37*, 94–102. [[CrossRef](#)] [[PubMed](#)]
10. Ha, D.; Hu, N.; Wu, C.; Kirsanov, D.; Legin, A.; Khaydukova, M.; Wang, P. Novel structured light-addressable potentiometric sensor array based on PVC membrane for determination of heavy metals. *Sens. Actuators B Chem.* **2012**, *174*, 59–64. [[CrossRef](#)]
11. Wan, H.; Sun, Q.; Li, H.; Sun, F.; Hu, N.; Wang, P. Design of a miniaturized multisensor chip with nanoband electrode array and light addressable potentiometric sensor for ion sensing. *Anal. Methods* **2015**, *7*, 9190–9197. [[CrossRef](#)]
12. Zhang, W.; Xu, Y.; Tahir, H.E.; Zou, X.; Wang, P. Rapid and wide-range determination of Cd(II), Pb(II), Cu(II) and Hg(II) in fish tissues using light addressable potentiometric sensor. *Food Chem.* **2017**, *221*, 541–547. [[CrossRef](#)] [[PubMed](#)]
13. Zhang, W.; Xu, Y.; Zou, X. Rapid determination of cadmium in rice using an all-solid RGO-enhanced light addressable potentiometric sensor. *Food Chem.* **2018**, *261*, 1–7. [[CrossRef](#)] [[PubMed](#)]
14. Lue, C.E.; Lai, C.S.; Wang, J.C.; Wu, C.M.; Yang, C.M. Differential Light Addressable Potentiometric Sensor with Poly(vinyl chloride) and HfO₂ Membranes for pH Sensors. *Jpn. J. Appl. Phys.* **2010**, *49*, 04DL10. [[CrossRef](#)]
15. DAS, A.; Das, A.; Chang, L.B.; Lai, C.S.; Lin, R.M.; Chu, F.C.; Lin, Y.H.; Chow, L.; Jeng, M.J. GaN Thin Film Based Light Addressable Potentiometric Sensor for pH Sensing Application. *Appl. Phys. Express* **2013**, *6*, 036601. [[CrossRef](#)]
16. Chin, C.H.; Lu, T.F.; Wang, J.C.; Yang, J.H.; Lue, C.E.; Yang, C.M.; Li, S.S.; Lai, C.S. Effects of CF₄ Plasma Treatment on pH and pNa Sensing Properties of Light-Addressable Potentiometric Sensor with a 2-nm-Thick Sensitive HfO₂ Layer Grown by Atomic Layer Deposition. *Jpn. J. Appl. Phys.* **2011**, *50*, 04DL06. [[CrossRef](#)]
17. Lue, C.E.; Lai, C.S.; Chen, H.Y.; Yang, C.M. Light Addressable Potentiometric Sensor with Fluorine-Terminated Hafnium Oxide Layer for Sodium Detection. *Jpn. J. Appl. Phys.* **2010**, *49*, 04DL05. [[CrossRef](#)]
18. Nose, K.; Miyamoto, K.-I.; Yoshinobu, T. Estimation of Potential Distribution during Crevice Corrosion through Analysis of I–V Curves Obtained by LAPS. *Sensors* **2020**, *20*, 2873. [[CrossRef](#)] [[PubMed](#)]
19. Lin, Y.H.; Das, A.; Lai, C.S. A Simple and Convenient Set-Up of Light Addressable Potentiometric Sensors (LAPS) for Chemical Imaging Using a Commercially Available Projector as a Light Source. *Int. J. Electrochem. Sci.* **2013**, *8*, 7062–7074.
20. Miyamoto, K.-I.; Wagner, T.; Yoshinobu, T.; Kanoh, S.; Schoening, M.J. Phase-mode LAPS and its application to chemical imaging. *Sens. Actuators B Chem.* **2011**, *154*, 28–32. [[CrossRef](#)]
21. Suzurikawa, J.; Nakao, M.; Kanzaki, R.; Takahashi, H. Microscale pH gradient generation by electrolysis on a light-addressable planar electrode. *Sens. Actuators B Chem.* **2010**, *149*, 205–211. [[CrossRef](#)]
22. Miyamoto, K.-I.; Kuwabara, Y.; Kanoh, S.; Yoshinobu, T.; Wagner, T.; Schöning, M.J. Chemical image scanner based on FDM-LAPS. *Sens. Actuators B Chem.* **2009**, *137*, 533–538. [[CrossRef](#)]
23. Miyamoto, K.; Wagner, T.; Mimura, S.; Kanoh, S.I.; Yoshinobu, T.; Schöning, M.J. Constant-phase-mode operation of the light-addressable potentiometric sensor. *Sens. Actuators B Chem.* **2011**, *154*, 119–123. [[CrossRef](#)]
24. Miyamoto, K.; Seki, K.; Guo, Y.; Wagner, T.; Schöning, M.J.; Yoshinobu, T. Enhancement of the Spatial Resolution of the Chemical Imaging Sensor by a Hybrid Fiber-Optic Illumination. *Procedia Eng.* **2014**, *87*, 612–615. [[CrossRef](#)]
25. Takenaga, S.; Schneider, B.; Erbay, E.; Biselli, M.; Schnitzler, T.; Schöning, M.J.; Wagner, T. Fabrication of bio-compatible lab-on-chip devices for biomedical applications by means of a 3D-printing process. *Phys. Status Solidi* **2015**, *212*, 1347–1352. [[CrossRef](#)]
26. Yang, J.H.; Lu, T.F.; Wang, J.C.; Lue, C.E.; Lai, C.S. Functionalization of nanoscaled 2 nm-thick ALD-HfO₂ layer by rapid thermal annealing and CF₄ plasma for LAPS NH₄⁺ detection. In Proceedings of the 2011 16th International Solid-State Sensors, Actuators and Microsystems Conference, Beijing, China, 5–9 June 2011; pp. 2118–2121.
27. Yang, J.-H.; Lu, T.-F.; Wang, J.-C.; Yang, C.-M.; Pijanowska, D.; Chin, C.H.; Lue, C.E.; Lai, C.S. LAPS with nanoscaled and highly polarized HfO₂ by CF₄ plasma for NH₄⁺ detection. *Sens. Actuators B Chem.* **2013**, *180*, 71–76. [[CrossRef](#)]
28. Wang, J.-C.; Ye, Y.-R.; Lin, Y.-H.; Johnson, D. Light-Addressable Potentiometric Sensor with Nitro-gen-Incorporated Ceramic Sm₂O₃ Membrane for Chloride Ions Detection. *J. Am. Ceram. Soc.* **2015**, *98*, 443–447. [[CrossRef](#)]
29. Liang, J.; Zhu, N.; Li, S.; Jia, H.; Xue, Y.; Cui, L.; Huang, Y.; Li, G. Light-addressable potentiometric sensor with gold nanoparticles enhancing enzymatic silver deposition for 1,5-anhydroglucitol determination. *Biochem. Eng. J.* **2017**, *123*, 29–37. [[CrossRef](#)]
30. Miyamoto, K.I.; Ichimura, H.; Wagner, T.; Schöning, M.J.; Yoshinobu, T. Chemical imaging of the concentration profile of ion diffusion in a microfluidic channel. *Sens. Actuators B Chem.* **2013**, *189*, 240–245. [[CrossRef](#)]
31. Chen, T.C.; Zeng, W.Y.; Liao, Y.H.; Das, A.; Yang, C.M.; Lai, C.-S. High photocurrent and operation frequency for light-addressable potentiometric sensor by thinner Si substrate. In Proceedings of the 2014 IEEE International Nanoelectronics Conference (INEC), Sapporo, Japan, 28–31 July 2014; pp. 1–3.
32. Wagner, T.; Werner, C.; Miyamoto, K.; Schöning, M.; Yoshinobu, T. A high-density multi-point LAPS set-up using a VCSEL array and FPGA control. *Procedia Chem.* **2009**, *1*, 1483–1486. [[CrossRef](#)]
33. Wan, H.; Ha, D.; Zhang, W.; Zhao, H.; Wang, X.; Sun, Q.; Wang, P. Design of a novel hybrid sensor with microelectrode array and LAPS for heavy metal determination using multivariate nonlinear calibration. *Sens. Actuators B Chem.* **2014**, *192*, 755–761. [[CrossRef](#)]
34. Cai, W.; Zhao, H.X.; Ha, D.; Guo, H.S.; Zhang, W.; Wang, P. Design of wireless sensor node based on a novel hybrid chemical sensor for heavy metal monitoring. In Proceedings of the 2011 16th International Solid-State Sensors, Actuators and Microsystems Conference, Beijing China, 5–9 June 2011; pp. 2114–2117.

35. Yoshinobu, T.; Schöning, M.J. Light-addressable potentiometric sensors for cell monitoring and biosensing. *Curr. Opin. Electrochem.* **2021**, *28*, 100727. [[CrossRef](#)]
36. Zeng, W.-Y.; Chen, C.-C.; Yang, C.-M.; Lai, C.-S. High photocurrent and high frequency response of light-addressable potentiometric sensor with thin Si substrate and surface roughness. In *2015 IEEE SENSORS*; IEEE: Pusan, Korea, 2015; pp. 1–3.
37. Yu, H.; Wang, J.; Liu, Q.; Zhang, W.; Cai, H.; Wang, P. High spatial resolution impedance measurement of EIS sensors for light addressable cell adhesion monitoring. *Biosens. Bioelectron.* **2011**, *26*, 2822–2827. [[CrossRef](#)]
38. Yang, C.-M.; Zeng, W.-Y.; Chen, Y.-P.; Chen, T.-C. Surface Modification for High Photocurrent and pH Sensitivity in a Silicon-Based Light-Addressable Potentiometric Sensor. *IEEE Sens. J.* **2018**, *18*, 2253–2259. [[CrossRef](#)]
39. Das, A.; Lin, Y.-H.; Lai, C.-S. Miniaturized amorphous-silicon based chemical imaging sensor system using a mini-projector as a simplified light-addressable scanning source. *Sens. Actuators B Chem.* **2014**, *190*, 664–672. [[CrossRef](#)]
40. Yang, C.M.; Liao, Y.H.; Chen, C.H.; Chen, C.C.; Lai, C.S. P-I-N Amorphous Silicon Light-Addressable Potentiometric Sensors for High-photovoltage Chemical Image. *Procedia Eng.* **2015**, *120*, 1015–1018. [[CrossRef](#)]
41. Zhou, B.; Das, A.; Kappers, M.J.; Oliver, R.A.; Humphreys, C.J.; Krause, S. InGaN as a Substrate for AC Photo-electrochemical Imaging. *Sensors* **2019**, *19*, 4386. [[CrossRef](#)]
42. Tu, Y.; Ahmad, N.; Briscoe, J.; Zhang, D.W.; Krause, S. Light-Addressable Potentiometric Sensors Using ZnO Nanorods as the Sensor Substrate for Bioanalytical Applications. *Anal. Chem.* **2018**, *90*, 8708–8715. [[CrossRef](#)]
43. Yang, C.M.; Liao, Y.H.; Chen, C.H.; Chen, T.C.; Lai, C.S.; Pijanowska, D. P-I-N amorphous silicon for thin-film light-addressable potentiometric sensors. *Sens. Actuators B Chem.* **2016**, *236*, 1005–1010. [[CrossRef](#)]
44. Chen, C.H.; Yang, C.M.; Chang, L.B.; Lai, C.S. Thickness effect of IGZO layer in light-addressable potentiometric sensor. In *Proceedings of the 2016 23rd International Workshop on Active-Matrix Flatpanel Displays and Devices (AM-FPD)*, Kyoto, Japan, 6–8 July 2016; pp. 203–205.
45. Siqueira, J.J.R.; Maki, R.M.; Paulovich, F.V.; Werner, C.F.; Poghossian, A.; de Oliveira, M.C.F.; Zucolotto, V.; Oliveira, J.O.N.; Schöning, M.J. Use of Information Visualization Methods Eliminating Cross Talk in Multiple Sensing Units Investigated for a Light-Addressable Potentiometric Sensor. *Anal. Chem.* **2009**, *82*, 61–65. [[CrossRef](#)]
46. Bratov, A.; Abramova, N.; Ipatov, A. Recent trends in potentiometric sensor arrays—A review. *Anal. Chim. Acta* **2010**, *678*, 149–159. [[CrossRef](#)] [[PubMed](#)]
47. Wang, J.; Zhou, Y.; Watkinson, M.; Gautrot, J.; Krause, S. High-sensitivity light-addressable potentiometric sensors using silicon on sapphire functionalized with self-assembled organic monolayers. *Sens. Actuators B Chem.* **2015**, *209*, 230–236. [[CrossRef](#)]
48. Yang, C.M.; Chiang, T.W.; Yeh, Y.T.; Das, A.; Lin, Y.T.; Chen, T.-C. Sensing and pH-imaging properties of niobium oxide prepared by rapid thermal annealing for electrolyte–insulator–semiconductor structure and light-addressable potentiometric sensor. *Sens. Actuators B Chem.* **2015**, *207*, 858–864. [[CrossRef](#)]
49. Wei, C.K.; Peng, H.-Y.; Tsai, Y.-C.; Chen, T.-C.; Yang, C.M. Fluorographene sensing membrane in a light-addressable potentiometric sensor. *Ceram. Int.* **2019**, *45*, 9074–9081. [[CrossRef](#)]
50. Yang, C.M.; Chen, C.-H.; Chang, L.B.; Lai, C.-S. IGZO Thin-Film Light-Addressable Potentiometric Sensor. *IEEE Electron Device Lett.* **2016**, *37*, 1481–1484. [[CrossRef](#)]
51. Yang, C.-M.; Yang, Y.-C.; Chen, C.-H. Thin-film light-addressable potentiometric sensor with SnOx as a photo-sensitive semiconductor. *Vacuum* **2019**, *168*, 108809. [[CrossRef](#)]
52. Suzurikawa, J.; Nakao, M.; Takahashi, H. Surface passivation of the thin-film LAPS with perhydropolysilazane-derived silica treated by O₂ plasma. *IEEJ Trans. Electr. Electron. Eng.* **2011**, *6*, 392–393. [[CrossRef](#)]
53. Suzurikawa, J.; Nakao, M.; Jimbo, Y.; Kanzaki, R.; Takahashi, H. A light addressable electrode with a TiO₂ nanocrystalline film for localized electrical stimulation of cultured neurons. *Sens. Actuators B Chem.* **2014**, *192*, 393–398. [[CrossRef](#)]
54. Litvinenko, S.; Kozinets, A.; Skryshevsky, V. Concept of photovoltaic transducer on a base of modified p–n junction solar cell. *Sens. Actuators A Phys.* **2015**, *224*, 30–35. [[CrossRef](#)]
55. Zhang, D.-W.; Wu, F.; Krause, S. LAPS and SPIM Imaging Using ITO-Coated Glass as the Substrate Material. *Anal. Chem.* **2017**, *89*, 8129–8133. [[CrossRef](#)]
56. Yue, Z.; Khalid, W.; Zanella, M.; Abbasi, A.Z.; Pfreundt, A.; Gil, P.R.; Schubert, K.; Lisdat, F.; Parak, W.J. Evaluation of quantum dots applied as switchable layer in a light-controlled electrochemical sensor. *Anal. Bioanal. Chem.* **2009**, *396*, 1095–1103. [[CrossRef](#)] [[PubMed](#)]
57. Chen, L.; Zhou, Y.; Krause, S.; Munoz, A.G.; Kunze, J.; Schmuiki, P. Repair of thin thermally grown silicon dioxide by anodic oxidation. *Electrochim. Acta* **2008**, *53*, 3395–3402. [[CrossRef](#)]
58. Zarei, L.; Tavallaie, R.; Choudhury, M.H.; Parker, S.G.; Bakthavathsalam, P.; Ciampi, S.; Gonçalves, V.R.; Gooding, J.J. DNA-Hybridization Detection on Si(100) Surfaces Using Light-Activated Electrochemistry: A Comparative Study between Bovine Serum Albumin and Hexaethylene Glycol as Antifouling Layers. *Langmuir* **2018**, *34*, 14817–14824. [[CrossRef](#)] [[PubMed](#)]
59. Wang, J.; Wu, F.; Watkinson, M.; Zhu, J.; Krause, S. "Click" Patterning of Self-Assembled Monolayers on Hydrogen-Terminated Silicon Surfaces and Their Characterization Using Light-Addressable Potentiometric Sensors. *Langmuir* **2015**, *31*, 9646–9654. [[CrossRef](#)] [[PubMed](#)]
60. Wang, J.; Campos, I.; Wu, F.; Zhu, J.; Sukhorukov, G.B.; Palma, M.; Watkinson, M.; Krause, S. The effect of gold nanoparticles on the impedance of microcapsules visualized by scanning photo-induced impedance microscopy. *Electrochim. Acta* **2016**, *208*, 39–46. [[CrossRef](#)]

61. Yang, C.-M.; Zeng, W.-Y.; Chen, C.-H.; Chen, Y.-P.; Chen, T.-C. Spatial resolution and 2D chemical image of light-addressable potentiometric sensor improved by inductively coupled-plasma reactive-ion etching. *Sens. Actuators B Chem.* **2018**, *258*, 1295–1301. [[CrossRef](#)]
62. Özsoylu, D.; Kizildag, S.; Schöning, M.J.; Wagner, T. Effect of Plasma Treatment on the Sensor Properties of a Light-Addressable Potentiometric Sensor (LAPS). *Phys. Status Solidi* **2019**, *216*, 1900259. [[CrossRef](#)]
63. Schöning, M.J.; Klock, J.P. About 20 Years of Silicon-Based Thin-Film Sensors with Chalcogenide Glass Materials for Heavy Metal Analysis: Technological Aspects of Fabrication and Miniaturization. *Electroanalysis* **2007**, *19*, 2029–2038. [[CrossRef](#)]
64. Zhang, D.-W.; Wu, F.; Wang, J.; Watkinson, M.; Krause, S. Image detection of yeast *Saccharomyces cerevisiae* by light-addressable potentiometric sensors (LAPS). *Electrochem. Commun.* **2016**, *72*, 41–45. [[CrossRef](#)]
65. Liu, J.; Jia, Y. Label-free protein chip and its detection system realization. In Proceedings of the 2011 IEEE International Conference of Electron Devices and Solid-State Circuits, Seoul, Korea, 7–10 August 2011; pp. 1–2.
66. Jia, Y.-F.; Gao, C.-Y.; He, J.; Feng, D.-F.; Xing, K.L.; Wu, M.; Liu, Y.; Cai, W.-S.; Feng, X.-Z. Unlabeled multi tumor marker detection system based on bioinitiated light addressable potentiometric sensor. *Analyst* **2012**, *137*, 3806–3813. [[CrossRef](#)] [[PubMed](#)]
67. Liang, J.; Guan, M.; Huang, G.; Qiu, H.; Chen, Z.; Li, G.; Huang, Y. Highly sensitive covalently functionalized light-addressable potentiometric sensor for determination of biomarker. *Mater. Sci. Eng. C* **2016**, *63*, 185–191. [[CrossRef](#)] [[PubMed](#)]
68. Jia, Y.; Yin, X.B.; Zhang, J.; Zhou, S.; Song, M.; Xing, K.L. Graphene oxide modified light addressable potentiometric sensor and its application for ssDNA monitoring. *Analyst* **2012**, *137*, 5866–5873. [[CrossRef](#)]
69. Bronder, T.; Wu, C.; Poghosian, A.; Werner, C.; Keusgen, M.; Schöning, M. Label-free Detection of DNA Hybridization with Light-addressable Potentiometric Sensors: Comparison of Various DNA-immobilization Strategies. *Procedia Eng.* **2014**, *87*, 755–758. [[CrossRef](#)]
70. Shao, C.; Zhou, S.; Yin, X.-B.; Gu, Y.; Jia, Y. Influences of Probe's Morphology for Metal Ion Detection Based on Light-Addressable Potentiometric Sensors. *Sensors* **2016**, *16*, 701. [[CrossRef](#)]
71. Khansili, N.; Rattu, G.; Krishna, P.M. Label-free optical biosensors for food and biological sensor applications. *Sens. Actuators B Chem.* **2018**, *265*, 35–49. [[CrossRef](#)]
72. Men, H.; Zou, S.; Li, Y.; Wang, Y.; Ye, X.; Wang, P. A novel electronic tongue combined MLAPS with stripping voltammetry for environmental detection. *Sens. Actuators B Chem.* **2005**, *110*, 350–357. [[CrossRef](#)]
73. Werner, C.F.; Groebel, S.; Krumb, C.; Wagner, T.; Selmer, T.; Yoshinobu, T.; Baumann, M.E.M.; Keusgen, M.; Schoening, M.J. Nutrient concentration-sensitive microorganism-based biosensor. *Phys. Status Solidi* **2012**, *209*, 900–904. [[CrossRef](#)]
74. Liu, Q.; Cai, H.; Xu, Y.; Li, Y.; Li, R.; Wang, P. Olfactory cell-based biosensor: A first step towards a neurochip of bioelectronic nose. *Biosens. Bioelectron.* **2006**, *22*, 318–322. [[CrossRef](#)]
75. Liu, Q.; Ye, W.; Yu, H.; Hu, N.; Du, L.; Wang, P.; Yang, M. Olfactory mucosa tissue-based biosensor: A bioelectronic nose with receptor cells in intact olfactory epithelium. *Sens. Actuators B Chem.* **2010**, *146*, 527–533. [[CrossRef](#)]
76. Liu, Q.; Ye, W.; Hu, N.; Cai, H.; Yu, H.; Wang, P. Olfactory receptor cells respond to odors in a tissue and semi-conductor hybrid neuron chip. *Biosens Bioelectron* **2010**, *26*, 1672–1678. [[CrossRef](#)] [[PubMed](#)]
77. Jia, Y.; Li, F.; Jia, T.; Wang, Z. Meso-tetra(4-carboxyphenyl)porphine-Enhanced DNA Methylation Sensing Interface on a Light-Addressable Potentiometric Sensor. *ACS Omega* **2019**, *4*, 12567–12574. [[CrossRef](#)] [[PubMed](#)]
78. Li, F.; Hu, S.; Zhang, R.; Gu, Y.; Li, Y.; Jia, Y. Porous Graphene Oxide Enhanced Aptamer Specific Circulating-Tumor-Cell Sensing Interface on Light Addressable Potentiometric Sensor: Clinical Application and Simulation. *ACS Appl Mater Interfaces* **2019**, *11*, 8704–8709. [[CrossRef](#)] [[PubMed](#)]
79. Jia, Y.; Li, F. Studies of Functional Nucleic Acids Modified Light Addressable Potentiometric Sensors: X-ray Photoelectron Spectroscopy, Biochemical Assay, and Simulation. *Anal. Chem.* **2018**, *90*, 5153–5161. [[CrossRef](#)] [[PubMed](#)]
80. Hu, W.J.; Cai, H.; Li, Y.; Li, R.; Wang, P.; Yang, G.G. Investigation of light addressable potentiometric sensor array sensitive to heavy metal ion based on micro-lens array. *J. Zhejiang Univ. Eng. Ing Sci.* **2008**, *42*, 517.
81. Jia, Y.; Gao, C.; Feng, D.; Wu, M.; Liu, Y.; Chen, X.; Xing, K.; Feng, X. Bio-initiated light addressable potentiometric sensor for unlabeled biodetection and its MEDICI simulation. *Analyst* **2011**, *136*, 4533–4538. [[CrossRef](#)] [[PubMed](#)]
82. Miyamoto, K.I.; Yoshida, M.; Sakai, T.; Matsuzaka, A.; Wagner, T.; Kanoh, S.I.; Yoshinobu, T.; Schöning, M.J. Differential Setup of Light-Addressable Potentiometric Sensor with an Enzyme Reactor in a Flow Channel. *Jpn. J. Appl. Phys.* **2011**, *50*, 04DL08. [[CrossRef](#)]
83. Zhang, W.; Liu, C.; Zou, X.; Zhang, H.; Xu, X. Micrometer-scale light-addressable potentiometric sensor on an optical fiber for biological glucose determination. *Anal. Chim. Acta* **2020**, *1123*, 36–43. [[CrossRef](#)] [[PubMed](#)]
84. Zhang, W.; Li, Y.; Liu, Q.; Xu, Y.; Cai, H.; Wang, P. A novel experimental research based on taste cell chips for taste transduction mechanism. *Sens. Actuators B Chem.* **2008**, *131*, 24–28. [[CrossRef](#)]
85. Liu, H.L.; Chen, Y.M.; Yang, M.C.; Lai, C.S. Real-time 2D pH images by fast scanning light-addressable Potentiometric sensor system controlled by LabVIEW program. *IEEE Sens.* **2015**, 1–3. [[CrossRef](#)]
86. Werner, C.F.; Takenaga, S.; Taki, H.; Sawada, K.; Schöning, M.J. Comparison of label-free ACh-imaging sensors based on CCD and LAPS. *Sens. Actuators B Chem.* **2013**, *177*, 745–752. [[CrossRef](#)]
87. Hu, N.; Ha, D.; Wu, C.; Zhou, J.; Kirsanov, D.; Legin, A.; Wang, P. A LAPS array with low cross-talk for non-invasive measurement of cellular metabolism. *Sens. Actuators A Phys.* **2012**, *187*, 50–56. [[CrossRef](#)]

88. Wang, J.; Yu, H.; Cai, H.; Du, L.P.; Liu, Q.J.; Wang, P. A photovoltage-based integrated sensor for nephrotoxicity evaluation under drug stimulation. In Proceedings of the 2011 16th International Solid-State Sensors, Actuators and Microsystems Conference, Beijing, China, 5–9 June 2011; pp. 2122–2125.
89. Hu, N.; Zhou, J.; Su, K.; Zhang, D.; Xiao, L.; Wang, T.; Wang, P. An integrated label-free cell-based biosensor for simultaneously monitoring of cellular physiology multiparameter in vitro. *Biomed. Microdevices* **2013**, *15*, 473–480. [[CrossRef](#)] [[PubMed](#)]
90. Yu, H.; Cai, H.; Zhang, W.; Xiao, L.; Liu, Q.; Wang, P. A novel design of multifunctional integrated cell-based biosensors for simultaneously detecting cell acidification and extracellular potential. *Biosens. Bioelectron.* **2009**, *24*, 1462–1468. [[CrossRef](#)] [[PubMed](#)]
91. Hu, N.; Wang, T.; Cao, J.; Su, K.; Zhou, J.; Wu, J.; Wang, P. Comparison between ECIS and LAPS for establishing a cardiomyocyte-based biosensor. *Sens. Actuators B Chem.* **2013**, *185*, 238–244. [[CrossRef](#)]
92. Wu, C.; Zhou, J.; Hu, N.; Ha, D.; Miao, X.; Wang, P. Cellular impedance sensing combined with LAPS as a new means for real-time monitoring cell growth and metabolism. *Sens. Actuators A Phys.* **2013**, *199*, 136–142. [[CrossRef](#)]
93. Dantism, S.; Röhlen, D.; Dahmen, M.; Wagner, T.; Wagner, P.; Schöning, M.J. LAPS-based monitoring of metabolic responses of bacterial cultures in a paper fermentation broth. *Sens. Actuators B Chem.* **2020**, *320*, 128232. [[CrossRef](#)]
94. Yoshinobu, T.; Miyamoto, K.; Wagner, T.; Schöning, M.J. Recent developments of chemical imaging sensor systems based on the principle of the light-addressable potentiometric sensor. *Sens. Actuators B Chem.* **2015**, *207*, 926–932. [[CrossRef](#)]
95. Dantism, S.; Takenaga, S.; Wagner, P.; Wagner, T.; Schöning, M.J. Determination of the extracellular acidification of *Escherichia coli* K12 with a multi-chamber-based LAPS system. *Phys. Status Solidi* **2016**, *213*, 1479–1485. [[CrossRef](#)]
96. Dantism, S.; Takenaga, S.; Wagner, T.; Wagner, P.; Schöning, M.J. Differential imaging of the metabolism of bacteria and eukaryotic cells based on light-addressable potentiometric sensors. *Electrochim. Acta* **2017**, *246*, 234–241. [[CrossRef](#)]
97. Su, K.; Zhou, J.; Zou, L.; Wang, T.; Zhuang, L.; Hu, N.; Wang, P. Integrated multifunctional cell-based biosensor system for monitoring extracellular acidification and cellular growth. *Sens. Actuators A Phys.* **2014**, *220*, 144–152. [[CrossRef](#)]
98. Dantism, S.; Takenaga, S.; Wagner, P.; Wagner, T.; Schöning, M. Light-addressable Potentiometric Sensor (LAPS) Combined with Multi-chamber Structures to Investigate the Metabolic Activity of Cells. *Procedia Eng.* **2015**, *120*, 384–387. [[CrossRef](#)]
99. Takenaga, S.; Herrera, C.; Werner, C.F.; Biselli, M.; Thönnessen, V.; Schnitzler, T.; Öhlschläger, P.; Almajhdi, F.N.; Wagner, T.; Schöning, M.J. Toward multi-analyte bioarray sensors: LAPS-based on-chip determination of a Michaelis-Menten-like kinetics for cell culturing. *Phys. Status Solidi* **2014**, *211*, 1410–1415. [[CrossRef](#)]
100. Liu, Q.; Hu, N.; Zhang, F.; Wang, H.; Ye, W.; Wang, P. Neurosecretory cell-based biosensor: Monitoring secretion of adrenal chromaffin cells by local extracellular acidification using light-addressable potentiometric sensor. *Biosens. Bioelectron.* **2012**, *35*, 421–424. [[CrossRef](#)] [[PubMed](#)]
101. Dantism, S.; Rohlen, D.; Selmer, T.; Wagner, T.; Wagner, P.; Schöning, M.J. Quantitative differential monitoring of the metabolic activity of *Corynebacterium glutamicum* cultures utilizing a light-addressable potentiometric sensor system. *Biosens. Bioelectron.* **2019**, *139*, 111332. [[CrossRef](#)]
102. Shaibani, P.M.; Etayash, H.; Naicker, S.; Kaur, K.; Thundat, T. Metabolic Study of Cancer Cells Using a pH Sensitive Hydrogel Nanofiber Light Addressable Potentiometric Sensor. *ACS Sens* **2017**, *2*, 151–156. [[CrossRef](#)]
103. Liang, T.; Gu, C.; Gan, Y.; Wu, Q.; He, C.; Tu, J.; Pan, Y.; Qiu, Y.; Kong, L.; Wan, H.; et al. Microfluidic chip system integrated with light addressable potentiometric sensor (LAPS) for real-time extracellular acidification detection. *Sens. Actuators B Chem.* **2019**, *301*, 127004. [[CrossRef](#)]
104. Liu, Q.; Yu, H.; Tan, Z.; Cai, H.; Ye, W.; Zhang, M.; Wang, P. In vitro assessing the risk of drug-induced cardio-toxicity by embryonic stem cell-based biosensor. *Sens. Actuators B Chem.* **2011**, *155*, 214–219. [[CrossRef](#)]
105. Kimmel, D.W.; Meschievitz, M.E.; Hiatt, L.A.; Cliffl, D.E. Multianalyte Microphysiometry of Macrophage Responses to Phorbol Myristate Acetate, Lipopolysaccharide, and Lipoarabinomannan. *Electroanalysis* **2013**, *25*, 1706–1712. [[CrossRef](#)]
106. Guo, Y.; Werner, C.F.; Handa, S.; Wang, M.; Ohshiro, T.; Mushiaki, H.; Yoshinobu, T. Miniature multiplexed label-free pH probe in vivo. *Biosens. Bioelectron.* **2021**, *174*, 112870. [[CrossRef](#)]
107. Guo, Y.; Werner, C.F.; Canales, A.; Yu, L.; Jia, X.; Anikeeva, P.; Yoshinobu, T. Polymer-fiber-coupled field-effect sensors for label-free deep brain recordings. *PLoS ONE* **2020**, *15*, e0228076. [[CrossRef](#)]
108. Jia, Y.; Qin, M.; Zhang, H.; Niu, W.; Li, X.; Wang, L.; Li, X.; Bai, Y.; Cao, Y.; Feng, X. Label-free biosensor: A novel phage-modified Light Addressable Potentiometric Sensor system for cancer cell monitoring. *Biosens. Bioelectron.* **2007**, *22*, 3261–3266. [[CrossRef](#)] [[PubMed](#)]
109. Shaibani, P.M.; Etayash, H.R.; Jiang, K.; Sohrabi, A.; Hassanpourfard, M.; Naicker, S.; Sadrzadeh, M.; Thundat, T. Portable Nanofiber-Light Addressable Potentiometric Sensor for Rapid *Escherichia coli* Detection in Orange Juice. *ACS Sens.* **2018**, *3*, 815–822. [[CrossRef](#)] [[PubMed](#)]
110. Shaibani, P.M.; Jiang, K.; Haghghat, G.; Hassanpourfard, M.; Etayash, H.; Naicker, S.; Thundat, T. The detection of *Escherichia coli* (*E. coli*) with the pH sensitive hydrogel nanofiber-light addressable potentiometric sensor (NF-LAPS). *Sens. Actuators B Chem.* **2016**, *226*, 176–183. [[CrossRef](#)]
111. Wagner, T.; Shigihara, N.; Miyamoto, K.; Suzurikawa, J.; Finger, F.; Schöning, M.J.; Yoshinobu, T. Light-addressable Potentiometric Sensors and Light-addressable Electrodes as a Combined Sensor-and-manipulator Microsystem with High Flexibility. *Procedia Eng.* **2012**, *47*, 890–893. [[CrossRef](#)]

112. Werner, C.F.; Krumb, C.; Schumacher, K.; Groebel, S.; Spelthahn, H.; Stellberg, M.; Wagner, T.; Yoshinobu, T.; Selmer, T.; Keusgen, M.; et al. Determination of the extracellular acidification of *Escherichia coli* by a light-addressable potentiometric sensor. *Phys. Status Solidi* **2011**, *208*, 1340–1344. [[CrossRef](#)]
113. Werner, C.F.; Wagner, T.; Miyamoto, K.-I.; Yoshinobu, T.; Schöning, M.J. High speed and high resolution chemical imaging based on a new type of OLED-LAPS set-up. *Sens. Actuators B Chem.* **2012**, *175*, 118–122. [[CrossRef](#)]
114. Itabashi, A.; Kosaka, N.; Miyamoto, K.I.; Wagner, T.; Schöning, M.J.; Yoshinobu, T. High-speed chemical imaging system based on front-side-illuminated LAPS. *Sens. Actuators B Chem.* **2013**, *182*, 315–321. [[CrossRef](#)]
115. Zhou, B.; Das, A.; Zhong, M.; Guo, Q.; Zhang, D.W.; Hing, K.A.; Sobrido, A.J.; Titirici, M.M.; Krause, S. Photoelectrochemical imaging system with high spatiotemporal resolution for visualizing dynamic cellular responses. *Biosens. Bioelectron.* **2021**, *180*, 113121. [[CrossRef](#)] [[PubMed](#)]
116. Miyamoto, K.; Seki, K.; Suto, T.; Werner, C.F.; Wagner, T.; Schöning, M.J.; Yoshinobu, T. Improved spatial resolution of the chemical imaging sensor with a hybrid illumination that suppresses lateral diffusion of photocarriers. *Sens. Actuators B Chem.* **2018**, *273*, 1328–1333. [[CrossRef](#)]
117. Werner, C.F.; Miyamoto, K.-I.; Wagner, T.; Schoening, M.J.; Yoshinobu, T. Lateral resolution enhancement of pulse-driven light-addressable potentiometric sensor. *Sens. Actuators B Chem.* **2017**, *248*, 961–965. [[CrossRef](#)]
118. Guo, Y.; Seki, K.; Miyamoto, K.I.; Wagner, T.; Schoening, M.J.; Yoshinobu, T. Novel photoexcitation method for light-addressable potentiometric sensor with higher spatial resolution. *Appl. Phys. Express* **2014**, *7*, 7. [[CrossRef](#)]
119. Miyamoto, K.I.; Kaneko, K.; Matsuo, A.; Wagner, T.; Kanoh, S.; Schoening, M.J.; Yoshinobu, T. Miniaturized chemical imaging sensor system using an OLED display panel. *Sens. Actuators B Chem.* **2012**, *170*, 82–87. [[CrossRef](#)]
120. Zhang, W.; Zhao, Y.; Ha, D.; Cai, W.; Wang, P. Light-addressable potentiometric sensor based on precise light intensity modulation for eliminating measurement error caused by light source. *Sens. Actuators A Phys.* **2012**, *185*, 139–144. [[CrossRef](#)]
121. Wagner, T.; Werner, C.F.B.; Miyamoto, K.I.; Schöning, M.J.; Yoshinobu, T. A high-density multi-point LAPS set-up using a VCSEL array and FPGA control. *Sens. Actuators B Chem.* **2011**, *154*, 124–128. [[CrossRef](#)]
122. Das, A.; Chen, T.-C.; Yang, C.-M.; Lai, C.-S. A high-speed, flexible-scanning chemical imaging system using a light-addressable potentiometric sensor integrated with an analog micromirror. *Sens. Actuators B Chem.* **2014**, *198*, 225–232. [[CrossRef](#)]
123. Lin, Y.H.; Das, A.; Ho, K.S.; Lai, C.S. A Novel Light-Addressable Potentiometric Sensors Set-Up with LCD Projector as Scanning Light Source. In Proceedings of the 2011 6th IEEE International Conference on Nano/Micro Engineered and Molecular Systems 2011, Kaohsiung, Taiwan, 20–23 February 2011; pp. 972–975.
124. Zhang, W.; Zhao, Y.; Ha, D.; Cai, W.; Wang, P. Design of precision light intensity modulation for light-addressable potentiometric sensor. In Proceedings of the 2011 16th International Solid-State Sensors, Actuators and Microsystems Conference, Beijing, China, 5–9 June 2011; pp. 1404–1407.
125. Wagner, T.; Werner, C.F.; Miyamoto, K.-I.; Schöning, M.J.; Yoshinobu, T. Development and characterisation of a compact light-addressable potentiometric sensor (LAPS) based on the digital light processing (DLP) technology for flexible chemical imaging. *Sens. Actuators B Chem.* **2012**, *170*, 34–39. [[CrossRef](#)]
126. Werner, C.F.; Schusser, S.; Spelthahn, H.; Wagner, T.; Yoshinobu, T.; Schöning, M.J. Field-programmable gate array based controller for multi spot light-addressable potentiometric sensors with integrated signal correction mode. *Electrochim. Acta* **2011**, *56*, 9656–9660. [[CrossRef](#)]
127. Wagner, K.; Miyamoto, C.F.; Werner, M.J.; Schöning; Yoshinobu, T. Flexible electrochemical imaging with “zoom-in” functionality by using a new type of light-addressable potentiometric sensor. In Proceedings of the 2011 16th International Solid-State Sensors, Actuators and Microsystems Conference, Beijing, China, 5–9 June 2011; pp. 2133–2135.
128. Wagner, T.; Werner, C.F.; Miyamoto, K.I.; Ackermann, H.J.; Yoshinobu, T.; Schöning, M.J.; Schoening, M.J. FPGA-based LAPS device for the flexible design of sensing sites on functional interfaces. *Phys. Status Solidi* **2010**, *207*, 844–849. [[CrossRef](#)]
129. Chen, L.; Zhou, Y.; Jiang, S.; Kunze, J.; Schmuki, P.; Krause, S. High resolution LAPS and SPIM. *Electrochem. Commun.* **2010**, *12*, 758–760. [[CrossRef](#)]
130. Chen, D.; Liu, S.-b.; Yin, S.-m.; Liang, J. Research on the enhancement of signal-to-noise ratio of light-addressable potentiometric sensor by optical focusing. *Optoelectron. Lett.* **2016**, *12*, 27–30. [[CrossRef](#)]
131. Dantism, S.; Röhlen, D.; Wagner, T.; Wagner, P.; Schöning, M.J. Optimization of Cell-Based Multi-Chamber LAPS Measurements Utilizing FPGA-Controlled Laser-Diode Modules. *Phys. Status Solidi* **2018**, *215*, 215. [[CrossRef](#)]